Article

SOURCE DATA | TRANSPARENT PROCESS

THE EMBO JOURNAL

The CatSper channel controls chemosensation in sea urchin sperm

Reinhard Seifert[1,2,†], Melanie Flick[1,†], Wolfgang Bönigk[1], Luis Alvarez[1], Christian Trötschel[3], Ansgar Poetsch[3], Astrid Müller[1], Normann Goodwin[2,4], Patric Pelzer[2,5], Nachiket D Kashikar[2,6], Elisabeth Kremmer[7], Jan Jikeli[1], Bernd Timmermann[8], Heiner Kuhl[8], Dmitry Fridman[1,2], Florian Windler[1,2], U Benjamin Kaupp[1,2,**] & Timo Strünker[1,2,*]

Abstract

Sperm guidance is controlled by chemical and physical cues. In many species, Ca^{2+} bursts in the flagellum govern navigation to the egg. In *Arbacia punctulata*, a model system of sperm chemotaxis, a cGMP signaling pathway controls these Ca^{2+} bursts. The underlying Ca^{2+} channel and its mechanisms of activation are unknown. Here, we identify CatSper Ca^{2+} channels in the flagellum of *A. punctulata* sperm. We show that CatSper mediates the chemoattractant-evoked Ca^{2+} influx and controls chemotactic steering; a concomitant alkalization serves as a highly cooperative mechanism that enables CatSper to transduce periodic voltage changes into Ca^{2+} bursts. Our results reveal intriguing phylogenetic commonalities but also variations between marine invertebrates and mammals regarding the function and control of CatSper. The variations probably reflect functional and mechanistic adaptations that evolved during the transition from external to internal fertilization.

Keywords CatSper; Ca^{2+} signaling; chemotaxis; sperm
Subject Categories Development & Differentiation; Membrane & Intracellular Transport
DOI 10.15252/embj.201489376 | Received 25 June 2014 | Revised 12 November 2014 | Accepted 21 November 2014 | Published online 22 December 2014
The EMBO Journal (2015) 34: 379–392

Introduction

The intracellular Ca^{2+} concentration ($[Ca^{2+}]_i$) coordinates several sperm functions required for fertilization (Ho & Suarez, 2001; Eisenbach & Giojalas, 2006; Florman *et al*, 2008; Kaupp *et al*, 2008; Publicover *et al*, 2008). In particular, Ca^{2+} controls the beat of the flagellum and, thereby, the swimming behavior. In mice and humans, the sperm-specific Ca^{2+} channel CatSper (cation channel of sperm) represents the principal pathway for Ca^{2+} entry into the flagellum (Quill *et al*, 2001; Ren *et al*, 2001; Kirichok *et al*, 2006; Lishko *et al*, 2010). Targeted disruption of CatSper in mice impairs sperm motility (Qi *et al*, 2007), and CatSper$^{-/-}$ sperm fail to traverse the oviduct (Ho *et al*, 2009; Miki & Clapham, 2013; Chung *et al*, 2014) and to penetrate the egg coat (Ren *et al*, 2001)—deficits that cause male infertility (Quill *et al*, 2001; Ren *et al*, 2001; Qi *et al*, 2007). Similarly, mutations in human CatSper genes cause infertility in men (Avenarius *et al*, 2009; Hildebrand *et al*, 2010).

CatSper has been proposed to serve as a polymodal sensor that integrates diverse chemical and physical cues (Brenker *et al*, 2012; Miki & Clapham, 2013; Tavares *et al*, 2013; Schiffer *et al*, 2014): In general, CatSper is activated at depolarized membrane potentials (V_m) and at alkaline intracellular pH (pH_i) (Kirichok *et al*, 2006; Lishko *et al*, 2010, 2011; Strünker *et al*, 2011). However, the interplay between V_m and pH_i to control CatSper during fertilization is unknown. In human sperm, hormones in the seminal fluid and the oviduct, i.e. prostaglandins and progesterone, directly activate CatSper (Lishko *et al*, 2011; Strünker *et al*, 2011; Brenker *et al*, 2012; Smith *et al*, 2013) and, thereby, affect sperm motility (Aitken & Kelly, 1985; Alasmari *et al*, 2013). Progesterone has been implicated in human sperm chemotaxis (Oren-Benaroya *et al*, 2008; Publicover *et al*, 2008; Teves *et al*, 2009); yet, *in vivo*, neither sperm chemotaxis nor the physiological role of these hormones during fertilization has been definitely established (Baldi *et al*, 2009). This is due to the demanding challenge to experimentally emulate the complex chemical, hydrodynamic, and topographical landscape of

1 Center of Advanced European Studies and Research (Caesar), Abteilung Molekulare Neurosensorik, Bonn, Germany
2 Marine Biological Laboratory, Woods Hole, MA, USA
3 Ruhr-Universität Bochum, Lehrstuhl Biochemie der Pflanzen, Bochum, Germany
4 Laboratory of Molecular Signalling, Babraham Institute, Cambridge, UK
5 Institut für Anatomie und Zellbiologie, Abteilung für Funktionelle Neuroanatomie, Universität Heidelberg, Heidelberg, Germany
6 Sussex Neuroscience, School of Life Sciences, University of Sussex, Falmer, Brighton, UK
7 Helmholtz-Zentrum München, Institut für Molekulare Immunologie, München, Germany
8 Max-Planck-Institut für Molekulare Genetik, Berlin, Germany
*Corresponding author. Tel: +49 228 9656 162; Fax: +49 228 9656 9162; E-mail: timo.struenker@caesar.de
**Corresponding author. Tel: +49 228 9656 100; Fax: +49 228 9656 9100; E-mail: u.b.kaupp@caesar.de
†These authors contributed equally to this work

the female genital tract (Suarez & Pacey, 2006; Suarez, 2008; Kirkman-Brown & Smith, 2011; Miki & Clapham, 2013).

In contrast, many aquatic species, in particular marine invertebrates, release their gametes into the ambient water; consequently, gametes of broadcast spawners can be studied under close to native conditions. For 100 years, sperm of marine invertebrates have served as a powerful model of fertilization research (Kaupp, 2012). It is well established that in the aquatic habitat, sperm are guided to the egg by chemotaxis. A case in point is sea urchin sperm. In sea urchin sperm, a cGMP signaling pathway generates Ca^{2+} bursts in the flagellum that coordinate chemotactic steering (Böhmer *et al*, 2005; Wood *et al*, 2005; Darszon *et al*, 2008; Kaupp *et al*, 2008; Guerrero *et al*, 2010a,b; Alvarez *et al*, 2012). Important components and cellular events of this signaling pathway have been identified (reviewed in Darszon *et al*, 2008; Kaupp *et al*, 2008; Alvarez *et al*, 2014). Briefly, the chemoattractant activates a receptor guanylyl cyclase (GC) and, thereby, stimulates rapid cGMP synthesis (Dangott & Garbers, 1984; Bentley *et al*, 1986, 1988; Shimomura & Garbers, 1986; Dangott *et al*, 1989; Kaupp *et al*, 2003). cGMP opens K^+-selective cyclic nucleotide-gated (CNGK) channels (Strünker *et al*, 2006; Galindo *et al*, 2007; Bönigk *et al*, 2009). The ensuing hyperpolarization (Cook & Babcock, 1993; Reynaud *et al*, 1993; Beltrán *et al*, 1996; Strünker *et al*, 2006) activates a sperm-specific voltage-dependent Na^+/H^+ exchanger (sNHE) (Lee, 1984a; Lee, 1984b; Lee & Garbers, 1986), mediating a rapid rise of pH_i (Nishigaki *et al*, 2001; Solzin *et al*, 2004) and, eventually, opens voltage-gated Ca^{2+} channels (Gonzáles-Martínez *et al*, 1992; Beltrán *et al*, 1996; Nishigaki *et al*, 2001; Kaupp *et al*, 2003; Strünker *et al*, 2006). However, to date, the molecular identity of the Ca^{2+} channel and its mechanism of activation have been elusive.

CatSper genes exist in many metazoan genomes, including aquatic animals (Cai & Clapham, 2008), yet the expression and function of CatSper in non-mammalian species are unknown. Here, we show that CatSper represents the long-sought Ca^{2+} channel of the chemotactic signaling pathway in sperm of the sea urchin *A. punctulata*. CatSper mediates the chemoattractant-induced Ca^{2+} bursts and controls chemotactic steering. We unveil the intimate, allosteric relationship between pH_i and V_m for CatSper activation: A minute chemoattractant-induced increase of pH_i enables CatSper in a highly cooperative fashion to open during a subsequent depolarization. The pH_i-induced shift of the voltage dependence of CatSper activation enables sperm to transduce periodic V_m changes into periodic Ca^{2+} bursts during sperm navigation on periodic paths in a chemoattractant gradient. We reveal intriguing commonalities and variations in the function and molecular makeup of chemosensory signaling pathways in sperm from mammals and marine invertebrates. Although different in design, these pathways share the CatSper channel as a key component of Ca^{2+} signaling.

Results

CatSper is expressed in the flagellum of *Arbacia punctulata* sperm

From a cDNA library of *A. punctulata* testis, we cloned four cDNAs encoding pore-forming CatSper subunits (*Ap*CatSper 1–4) (Fig 1A, Supplementary Fig S1). Each *Ap*CatSper subunit harbors six transmembrane segments (S1–S6), a voltage sensor in S4, and a pore loop between S5 and S6 (Fig 1A, Supplementary Fig S1). The pore loops carry the signature sequence of Ca_v and CatSper channels (Fig 1B, upper panel) (Navarro *et al*, 2008). Similar to other voltage-gated channels, the S4 segments of all four *Ap*CatSper subunits carry six to seven positively charged residues (Fig 1B, lower panel). The intracellular N- or C-termini of *Ap*CatSper 1, 2, and 4, but not of *Ap*CatSper 3, carry coiled-coil domains (Fig 1A, Supplementary Fig S1) that were proposed to mediate heterotetramerization in mammalian CatSper (Lobley *et al*, 2003). The overall homology of *Ap*CatSper subunits with their mammalian CatSper ortholog is low (25–35%).

To localize *Ap*CatSper subunits in sperm, we raised monoclonal antibodies against *Ap*CatSper 2 and 3 (Supplementary Fig S1). Hemagglutinin (HA)-tagged *Ap*CatSper 2 and 3 subunits were heterologously expressed in Chinese hamster ovary (CHO) cells. In Western blots, an anti-HA antibody labeled polypeptides with apparent molecular weights (M_w) of 66.5 ± 3.1 kDa (*Ap*CatSper 2, $n = 24$) and 41.6 ± 2.1 kDa (*Ap*CatSper 3, $n = 9$). The same polypeptides were recognized by the monoclonal anti-*Ap*CatSper 2 and 3 antibodies in transfected CHO cells and in sperm (Fig 1C), demonstrating that *Ap*CatSper 2 and 3 are expressed in *A. punctulata* sperm. In immunocytochemistry, the anti-*Ap*CatSper 3 antibody stained the flagellum (Fig 1D, left). The staining pattern of the receptor GC (Fig 1D, middle), the CNGK channel (Fig 1D, right), and *Ap*CatSper 3 overlapped, showing that CatSper colocalizes with components of the chemotactic signaling pathway. Mass spectrometry confirmed the presence of *Ap*CatSper 1–4 in the flagellum: In protein preparations from purified flagella, we identified proteotypic peptides for all four *Ap*CatSper subunits (Supplementary Fig S1, Supplementary Table S1); the peptides covered 5–25% of the respective protein sequences (Supplementary Table S1). Moreover, in the *A. punctulata* genome and testis transcriptome (to be published), we identified a gene encoding the accessory subunit CatSper δ (Chung *et al*, 2011) and mRNAs encoding CatSper β (Liu *et al*, 2007) and CatSper γ (Wang *et al*, 2009) (Supplementary Fig S1, Fig 1A). In purified flagella, we identified proteotypic peptides of the predicted accessory subunits (Supplementary Table S1). We conclude that *Ap*CatSper 1–4 and *Ap*CatSper β, δ, and γ are expressed in sperm and are located in the flagellum.

We immunoprecipitated *Ap*CatSper 2 and *Ap*CatSper 3, using the respective anti-*Ap*CatSper antibodies. Analysis of the co-immunoprecipitates by Western blotting (Fig 1E) and mass spectrometry (Fig 1F, Supplementary Table S2) indicates that *Ap*CatSper 1–4, β, δ, and γ interact to form a protein complex. Therefore, we propose that the architecture of the CatSper channel is similar in sea urchins and mammals. Unfortunately, like their mammalian counterparts (Ren *et al*, 2001), heterologously expressed *Ap*CatSper subunits did not yield functional channels.

Intracellular pH and membrane voltage control Ca^{2+} influx in sea urchin sperm

Using a stopped-flow apparatus and fluorescent probes for Ca^{2+}, V_m, and pH, we studied the role of CatSper in intact *A. punctulata* sperm. Ammonium chloride (NH_4Cl) evoked a rapid and sustained intracellular alkalization (Supplementary Fig S2) that stimulated a Ca^{2+} increase (Fig 2A). At low NH_4Cl concentrations (≤ 3 mM),

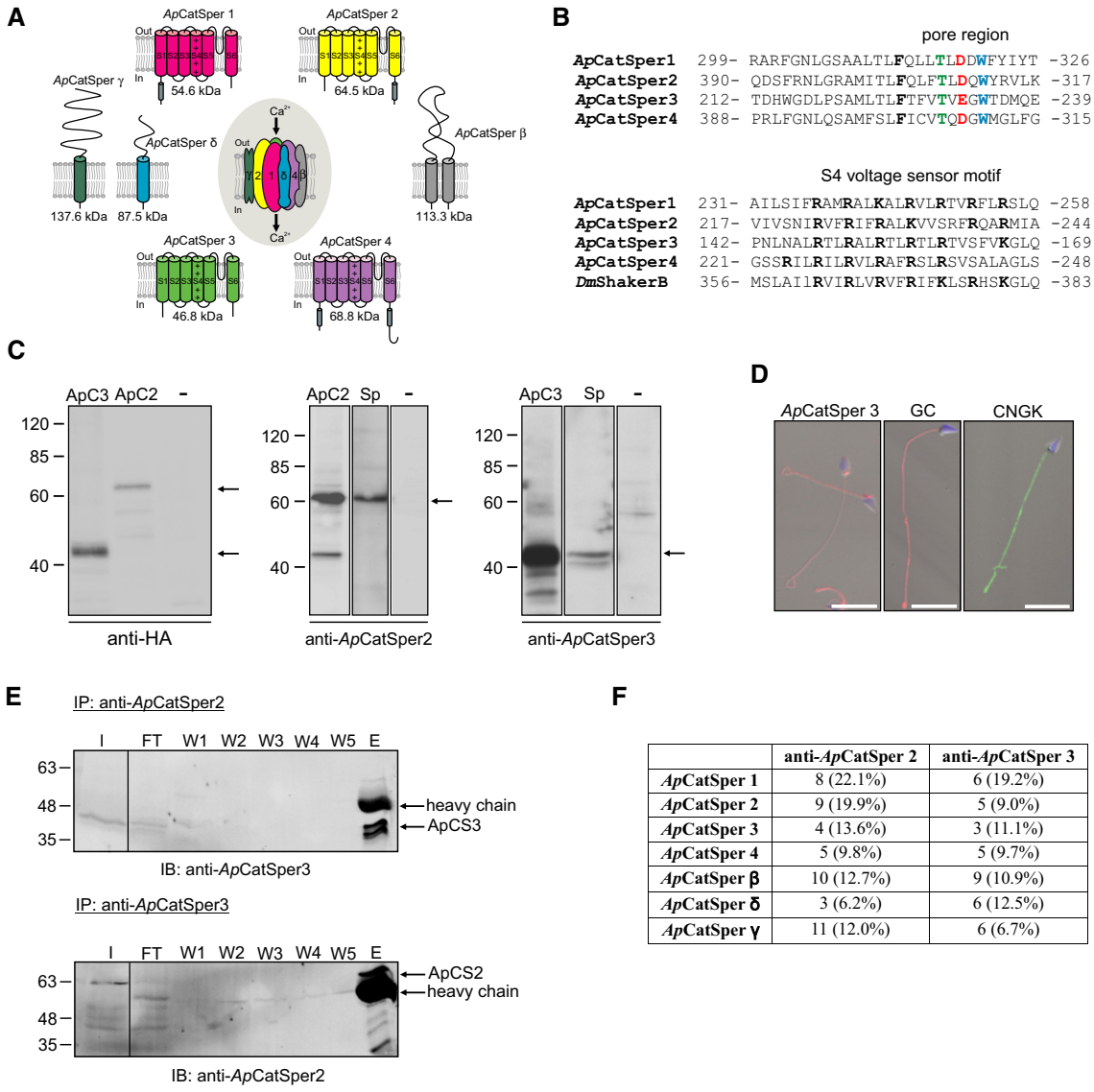

	anti-*Ap*CatSper 2	anti-*Ap*CatSper 3
***Ap*CatSper 1**	8 (22.1%)	6 (19.2%)
***Ap*CatSper 2**	9 (19.9%)	5 (9.0%)
***Ap*CatSper 3**	4 (13.6%)	3 (11.1%)
***Ap*CatSper 4**	5 (9.8%)	5 (9.7%)
***Ap*CatSper β**	10 (12.7%)	9 (10.9%)
***Ap*CatSper δ**	3 (6.2%)	6 (12.5%)
***Ap*CatSper γ**	11 (12.0%)	6 (6.7%)

Figure 1. Features of *Ap*CatSper 1–4, β, γ, and δ and localization of CatSper in *A. punctulata* sperm.

A Predicted membrane topology and predicted molecular weight of *Ap*CatSper 1–4 cloned from *A. punctulata* testis, and of *Ap*CatSper β, δ, and γ. A gene encoding *Ap*CatSper δ was identified in the *A. punctulata* genome; transcripts encoding *Ap*CatSper β and *Ap*CatSper γ were identified in the *A. punctulata* transcriptome. S1 to S6, transmembrane segments; +, positively charged amino acids in S4; gray cylinder, coiled-coil domain.

B Upper panel, alignment of pore regions of *Ap*CatSper 1–4. Amino acids of the Ca^{2+} selectivity-filter motif are highlighted. Lower panel, alignment of S4 voltage-sensor segments of *Ap*CatSper 1–4 and of *D. melanogaster* ShakerB K_v channel. Positively charged amino acids are highlighted. Numbers indicate start and end position of amino acids of the selected region.

C Western blots of total protein of CHO cells transfected with *Ap*CatSper 2 or 3, non-transfected control cells (-), and *A. punctulata* sperm (Sp). The Western blots were probed with anti-HA, anti-*Ap*CatSper 2, or anti-*Ap*CatSper 3 antibodies. Arrows indicate bands representing *Ap*CatSper 2 and 3.

D Immunocytochemical analysis of sperm stained with anti-*Ap*CatSper 3, anti-GC, or anti-CNGK antibodies; superposition of images obtained by fluorescence and bright-field microscopy; scale bar = 10 μm. The DNA was stained with DAPI (blue).

E Western blot analysis of co-immunoprecipitation (IP) of *A. punctulata* sperm proteins. The input (I), flow through (FT), washes (W1-5), and the eluate (E) of the IP using the anti-*Ap*CatSper 2 antibody were probed with the anti-*Ap*CatSper 3 antibody (upper panel) and vice versa (lower panel). *Ap*CatSper 3 and *Ap*CatSper 2 were co-immunoprecipitated with the anti-*Ap*CatSper 2 (upper panel) and anti-*Ap*CatSper 3 antibody (lower panel), respectively.

F Analysis by mass spectrometry of immunoprecipitated proteins. *Ap*CatSper 1-4, β, γ, and δ were identified in the immunoprecipitates obtained with both the anti-*Ap*CatSper 2 and anti-*Ap*CatSper 3 antibodies. The number of tryptic peptides identified and the respective sequence coverage are given.

Source data are available online for this figure.

Ca^{2+} signals slowly reached a plateau; at higher concentrations (≥ 10 mM), NH_4Cl evoked rapid, oscillatory Ca^{2+} responses (Fig 2A). Mixing of sperm with both NH_4Cl and EGTA, which lowers extracellular [Ca^{2+}] to ≤ 400 nM, abolished the Ca^{2+}, but not the pH_i response (Supplementary Fig S2), demonstrating that alkalization stimulates Ca^{2+} influx.

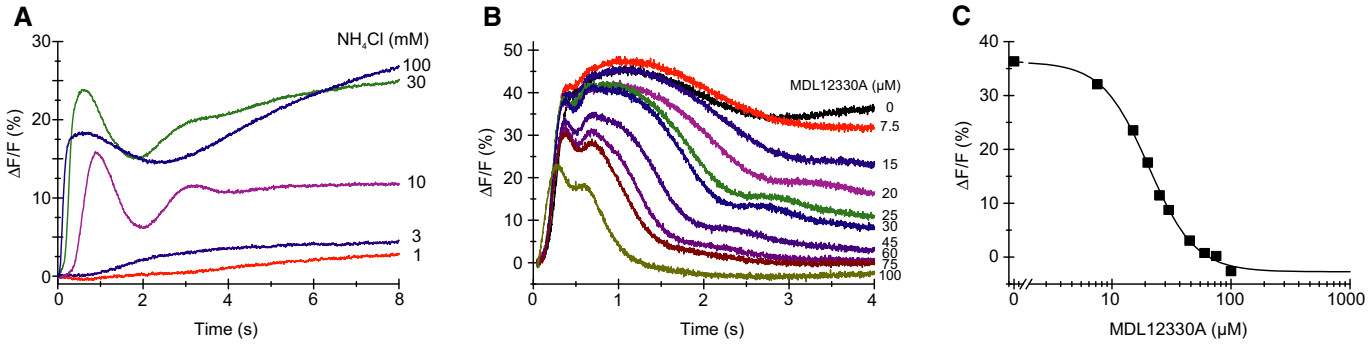

Figure 2. CatSper inhibitors abolish alkaline-evoked Ca^{2+} influx in *A. punctulata* sperm.

A Alkaline-evoked Ca^{2+} signals in sperm mixed with NH_4Cl; sperm were loaded with the Ca^{2+} indicator Fluo-4. ΔF/F (%) indicates the change in Fluo-4 fluorescence (ΔF) with respect to the basal fluorescence (F, mean of the first 3–5 data points).

B Ca^{2+} signals evoked by mixing of sperm simultaneously with NH_4Cl (30 mM) and the CatSper inhibitor MDL12330A.

C Dose–response relation of inhibition of the Ca^{2+} signals shown in panel (B), K_i = 20 μM, amplitudes were determined at t = 4 s.

Two distinct CatSper inhibitors, MDL12330A (MDL) (Brenker *et al*, 2012) and mibefradil (Strünker *et al*, 2011), suppressed the alkaline-evoked Ca^{2+} signal (Fig 2B and C, Supplementary Fig S2); the constants of half-maximal inhibition (K_i) were 15.6 ± 3.3 μM (MDL) and 20.7 ± 5.1 μM (mibefradil) (n = 4) (Fig 2B and C, Supplementary Fig S2). Sperm were mixed simultaneously with NH_4Cl and the inhibitors, and the time course of inhibition probably reflects the time required for the drug to reach the blocking site; we did not test whether drug action reached steady state within the recording time.

The drugs inhibit CatSper-mediated Ca^{2+} signals in human sperm with similar potency (Strünker *et al*, 2011; Brenker *et al*, 2012). We conclude that in sea urchin sperm, similar to mouse and human sperm, CatSper mediates alkaline-evoked Ca^{2+} influx. Because MDL and mibefradil are not selective for CatSper, we cannot exclude that the sperm might harbor additional, so far unknown Ca^{2+}-permeable channels that are also activated at alkaline pH_i and inhibited by both drugs.

We determined the pH_i sensitivity of the alkaline-induced Ca^{2+} influx using the "pH_i pseudo-null-point" method (Eisner *et al*, 1989; Chow *et al*, 1996; Bond & Varley, 2005; Swietach *et al*, 2010) that allows clamping of pH_i to fixed values and calibration of the pH indicator BCECF. Key is a set of pH_i-clamp solutions composed of a weak acid (butyric acid, BA) and a weak base (trimethylamine, TMA) at different molar ratios (see Materials and Methods). TMA and BA freely equilibrate across the membrane and, at sufficiently high concentrations (see Materials and Methods), establish a defined pH_i that is set by the acid/base ratio (Chow *et al*, 1996).

Mixing of sperm with a pH_i 7.2-clamp solution changed pH_i only slightly, suggesting a resting pH (pH_{rest}) of about 7.2 (Fig 3A). Mixing with pH_i-clamp solutions < 7.2 and > 7.2 evoked acidification and alkalization, respectively, that was stable after 4–5 s and persisted for at least 14 s (Fig 3A). The changes in ΔR/R of BCECF fluorescence were linearly related to pH_i-clamp values (Fig 3B); interpolation yielded a pH_{rest} of 7.16 ± 0.04 (Fig 3B; n = 7). Similar pH_{rest} values of sea urchin sperm were determined by other methods (Babcock *et al*, 1992; Guerrero *et al*, 1998). Moreover, the calibration allowed rescaling of the data in Fig 3A to absolute pH_i values (inset in Fig 3B).

Figure 3C shows the time course of Ca^{2+} responses in sperm mixed with different pH_i-clamp solutions. Plotting the amplitude of the Ca^{2+} signals versus the respective pH_i-clamp values disclosed an exceptionally steep dose–response relation with a $pH_{½}$ of 7.47 ± 0.01 and a Hill coefficient of 10.8 ± 2.2 (Fig 3D, n = 4). From the time course of the changes in pH_i and Ca^{2+}, we reconstructed the threshold pH_i (pH_{thr}) at which the Ca^{2+} influx commenced (Fig 3E). For example, using the pH_i 7.6-clamp solution, the Ca^{2+} signal was observed after a latency of ≅ 200 ms (Fig 3E, dotted black line), at which the pH_i of sperm had increased to ≅ 7.3 (Fig 3E, dotted red line), i.e. pH_{thr} for Ca^{2+} influx. We determined pH_{thr} for the entire range of pH_i-clamp solutions (Fig 3F). The latency of the Ca^{2+} influx decreased with increasing pH_i-clamp values (Fig 3F, black), because the alkalization proceeded on a faster time scale (Fig 3A and inset of Fig 3B). However, pH_{thr} was largely independent of the rate and magnitude of the pH_i increase (Fig 3F, red). The invariant pH_{thr} for the alkaline-induced Ca^{2+} influx and its exceptionally steep, switch-like dose–response relation suggest that intracellular alkalization sensitizes CatSper to open during depolarization.

We also wondered whether depolarization evokes a Ca^{2+} increase. In fact, rapid elevation of the extracellular K^+ concentration ($[K^+]_o$) to ≥ 30 mM evoked a transient Ca^{2+} signal (Fig 4A), whose amplitude was graded with $[K^+]_o$. MDL inhibited Ca^{2+} signals evoked by 80 mM and 160 mM K^+ with a K_i of 38.8 ± 7.5 μM and 29.2 ± 11.2 μM (n = 3), respectively (Fig 4B–D); the Ca^{2+} signals were also suppressed by mibefradil (Supplementary Fig S2). We conclude that CatSper also supports depolarization-evoked Ca^{2+} influx in sea urchin sperm.

We examined the relationship between pH_{thr} and V_m. To manipulate the resting potential (V_{rest}), sperm were incubated at different $[K^+]_o$. In standard artificial sea water (ASW, 9 mM $[K^+]_o$), V_{rest} was −51.9 ± 2 mV (Fig 4E, n = 6); sperm were hyperpolarized and depolarized to −54.9 ± 2.2 mV and −26.3 ± 4.2 mV, respectively, at low (3 mM) and high (191 mM) $[K^+]_o$ (Fig 4F, n = 3); V_{rest} was determined by the $[K^+]_o$ null-point method (Strünker *et al*, 2006; see also Materials and Methods), assuming an intracellular K^+ concentration of 423 mM. Probing cells with different pH_i-clamp solutions and analyzing the time course of pH_i and Ca^{2+} signals

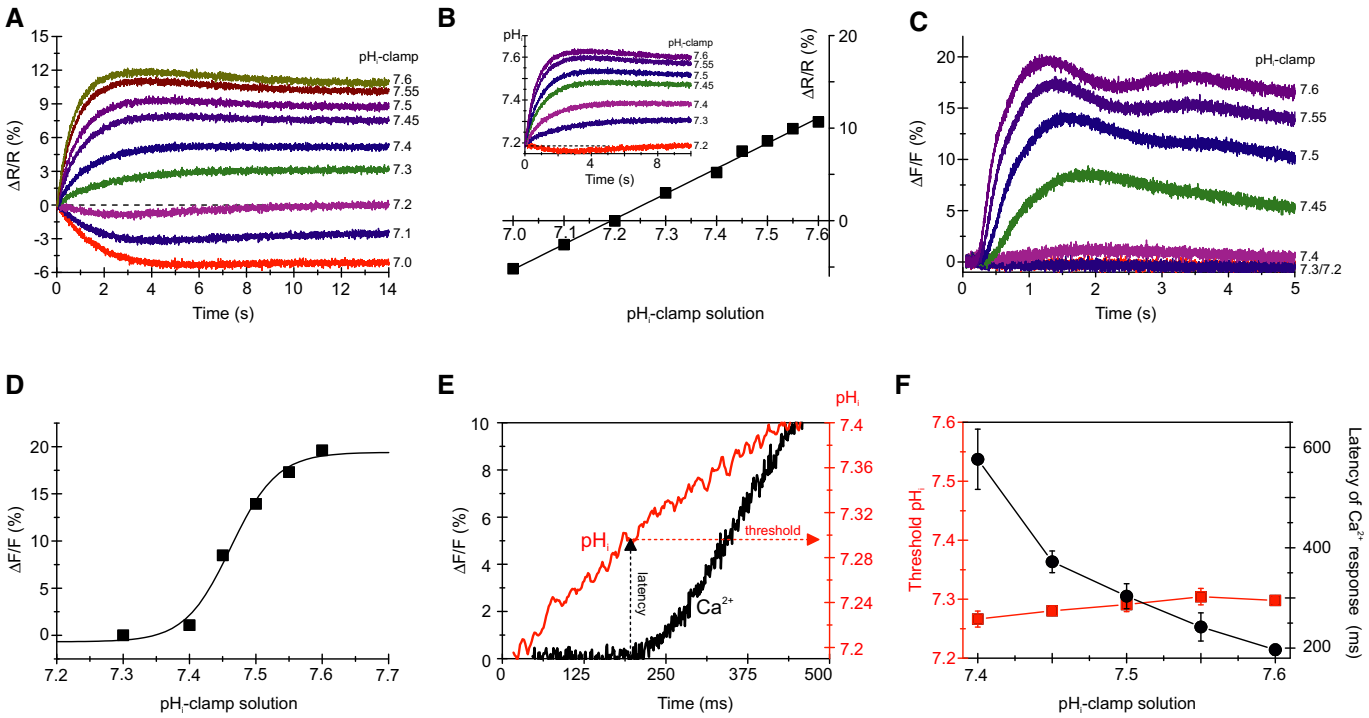

Figure 3. Determination of the threshold pH_i for alkaline-evoked Ca^{2+} influx.

A Changes in pH_i evoked by mixing with pH_i-clamp solutions (see explanation in the text); sperm were loaded with the pH_i indicator BCECF. $\Delta R/R$ (%) indicates the change in the BCECF fluorescence emission ratio ($\Delta R = F_{494}/F_{540}$) with respect to the basal ratio (R, mean of the first 3–5 data points).

B Steady-state change (at t = 14 s) of BCECF fluorescence for the pH_i signals shown in (A). The intercept of the fitted straight line with the x-axis yields the resting pH_i; the slope of the straight line yields the $\Delta R/R$ (%) × ΔpH^{-1}. Inset: calibrated changes in pH_i evoked by various pH_i-clamp solutions.

C Ca^{2+} signals evoked by mixing of sperm with pH_i-clamp solutions.

D Dose–response relation for the Ca^{2+} signals shown in (C).

E Calibrated pH_i increase (red) and respective Ca^{2+} response (black) evoked by mixing of sperm with a pH_i 7.6-clamp solution; depicted are, on an extended time scale, the first 500 ms of the respective pH_i increase and Ca^{2+} signal shown in (B, inset) and (C), respectively. The threshold pH_i for CatSper activation was deduced from the latency of the Ca^{2+} signal.

F Threshold pH_i and latency of Ca^{2+} signals evoked by various pH_i-clamp solutions (mean ± SD; $n \geq 3$).

revealed pH_{thr} for different V_{rest} values (Fig 4E, Supplementary Fig S3). At hyperpolarized V_{rest}, the pH_{thr} for Ca^{2+} influx was shifted to more alkaline pH_i values (Fig 4E, Supplementary Fig S3); when V_{rest} was depolarized, the pH_{thr} was shifted to more acidic pH_i values (Fig 4E and F, Supplementary Fig S3); a linear fit of the data yielded a slope of ΔpH_{thr}/10 mV of 0.07 ± 0.004 (standard error of the fit) (Fig 4F, red line). In addition, pH_{rest} was more acidic at depolarized V_{rest} (Fig 4F). We conclude that the control of Ca^{2+} influx via CatSper by pH_i and membrane voltage is closely intertwined.

Chemoattractant-induced ΔpH_i and ΔV_m orchestrate Ca^{2+} influx in sea urchin sperm

We studied the control of Ca^{2+} influx by pH_i and V_m in sperm stimulated with either the chemoattractant resact or the intracellular messenger cGMP. Ca^{2+} signals evoked by photorelease of resact from caged resact were abolished by MDL (K_i = 6.4 ± 1 μM) and mibefradil (9.5 ± 1.6 μM) (n = 3) (Fig 5A, C, and D, Supplementary Fig S4). Both drugs also abolished Ca^{2+} signals evoked by intracellular photorelease of cGMP from caged cGMP (MDL: K_i = 3.9 ± 0.4 μM; mibefradil: K_i = 25.2 ± 3.7 μM) (n = 3) (Fig 5B–D, Supplementary Fig S4). The potency of MDL to inhibit the resact- and cGMP-evoked Ca^{2+} responses was about 2- to 3-fold higher than the potency to inhibit Ca^{2+} signals evoked by alkalization or depolarization. However, sperm were first pre-incubated for about 5 s before resact or cGMP was released. This short pre-incubation might enhance the potency. It is however unclear, why mibefradil inhibited the resact- and cGMP-induced Ca^{2+} responses with about 3-fold different potencies. Altogether, we conclude that CatSper mediates the chemoattractant- and cGMP-induced Ca^{2+} influx.

Resact and cGMP stimulate a transient hyperpolarization, and the Ca^{2+} influx commences shortly after the hyperpolarization peaks (Strünker *et al*, 2006). Moreover, resact and cGMP also evoke a rapid pH_i increase (Fig 6D, Supplementary Fig S5) (Darszon *et al*, 2008). Given the steep pH_i sensitivity of the alkaline-evoked Ca^{2+} influx, we scrutinized the hypothesis that the pH_i increase allosterically shifts the voltage dependence of CatSper to more negative V_m values. A prerequisite for such a mechanism is that the onset of ΔpH_i precedes the onset of the Ca^{2+} signal. Therefore, we determined the exact timing and sequence of signaling events for resact concentrations ranging from 500 fM to 25 nM (Fig 6A, Supplementary Fig S6). For all concentrations, the sequence of cellular events

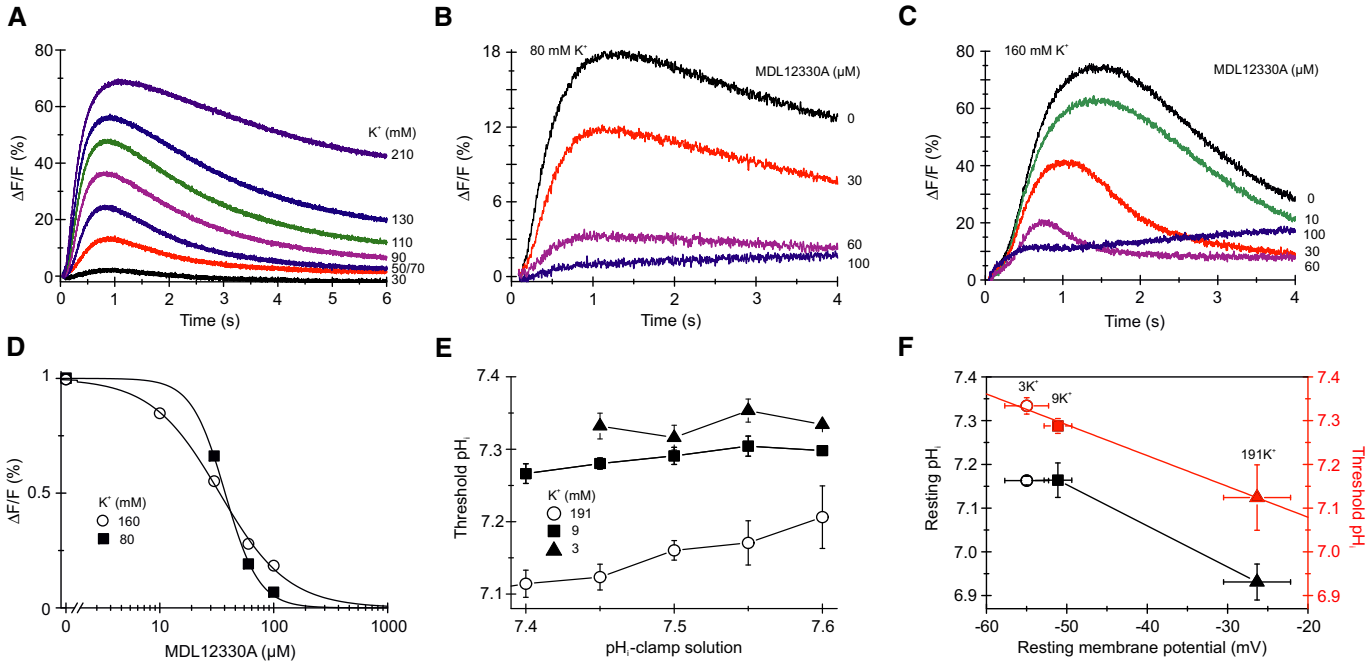

Figure 4. The threshold pH_i for alkaline-evoked Ca^{2+} influx is controlled by V_m.

A Depolarization-evoked Ca^{2+} signals in sperm mixed with ASW containing high KCl concentrations.

B Ca^{2+} signals evoked by mixing of sperm with 80 mM KCl and the CatSper inhibitor MDL12330A.

C Ca^{2+} signals evoked by mixing of sperm with 160 mM KCl and MDL12330A.

D Dose–response relation for the Ca^{2+} signals shown in (B, C) at t = 1–2 s.

E Threshold pH_i for Ca^{2+} signals evoked by pH_i-clamp solutions in sperm bathed in ASW containing low (3 mM), high (191 mM), and normal (9 mM) KCl (mean ± SD; $n \geq 3$); data for 9 mM KCl are from Fig 3F.

F Resting pH_i and resting V_m in sperm bathed in ASW containing low (3 mM), high (191 mM), and normal (9 mM) KCl (black) (mean ± SD; $n \geq 3$). Mean threshold pH_i for CatSper activation at different membrane potentials (red); mean threshold pH_i was derived from data shown in (E).

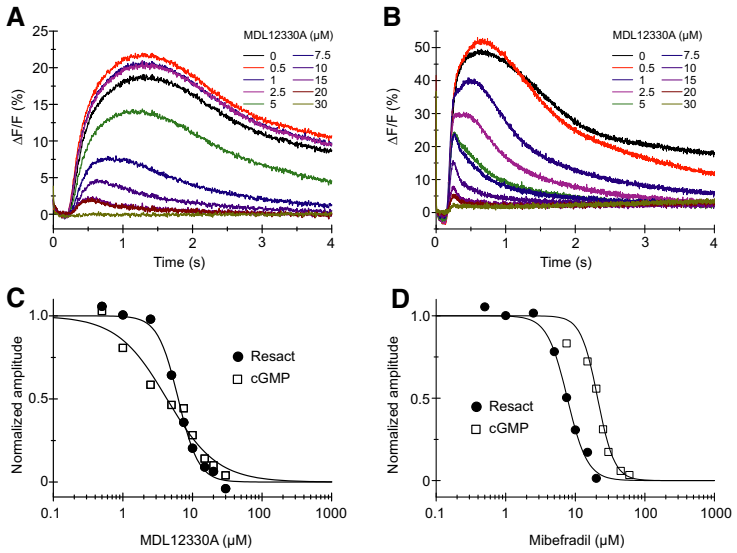

Figure 5. CatSper inhibitors abolish chemoattractant- and cGMP-induced Ca^{2+} influx.

A Ca^{2+} signals in sperm evoked by photorelease (at t = 0) of resact from caged resact in the presence of the CatSper inhibitor MDL12330A.

B Ca^{2+} signals evoked by intracellular photorelease (at t = 0) of cGMP in sperm loaded with caged cGMP in the presence of the CatSper inhibitor MDL12330A.

C Normalized dose–response relation for inhibition of the resact- and cGMP-induced Ca^{2+} signals shown in (A, B) (K_i = 6.2 and 4.3 μM, respectively).

D Normalized dose–response relation for inhibition of the resact- and cGMP-induced Ca^{2+} signals shown in Supplementary Fig S4 by the CatSper inhibitor mibefradil (K_i = 7.7 and 20.9 μM, respectively).

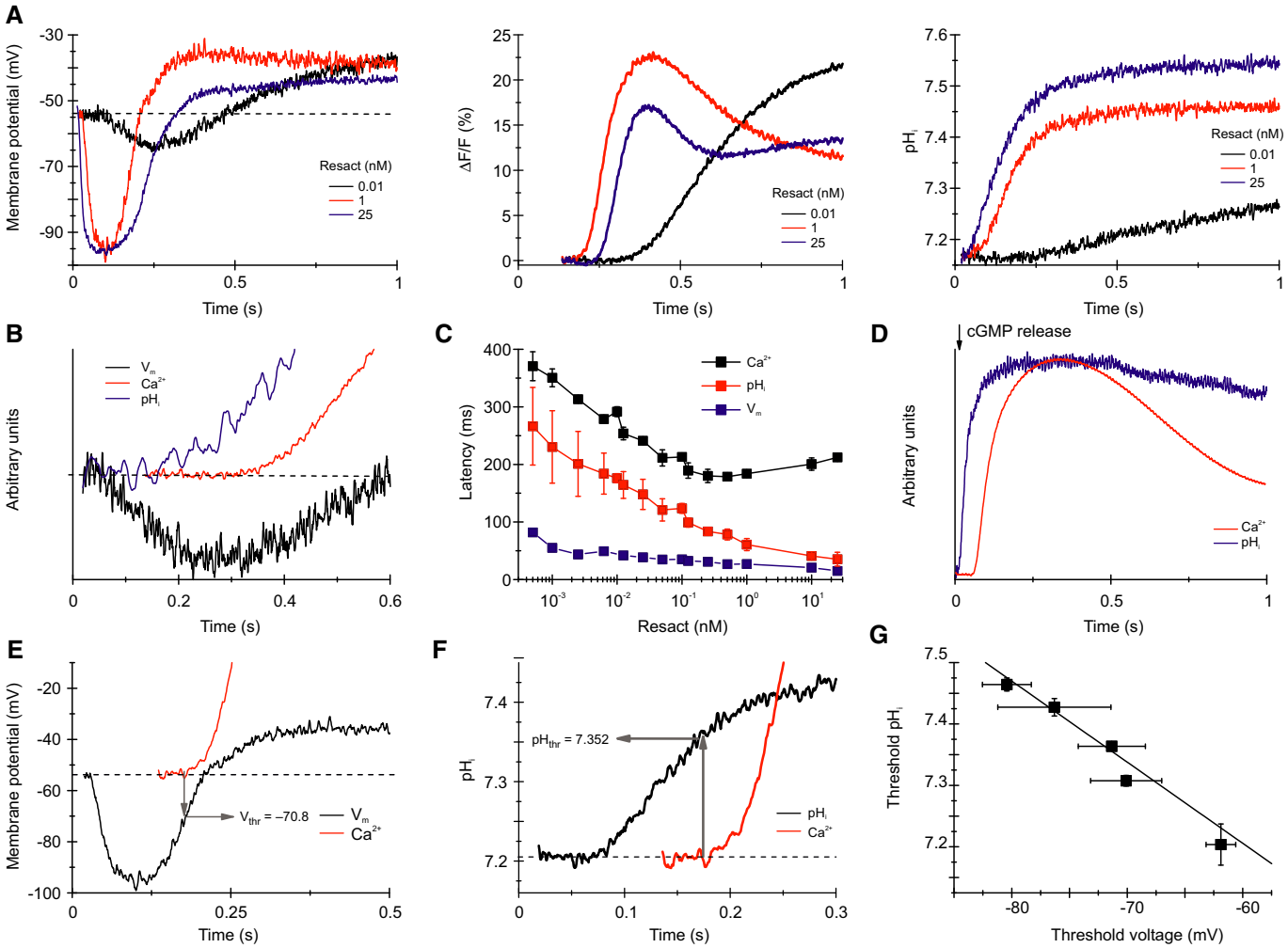

Figure 6. The chemoattractant-induced Ca^{2+} influx is orchestrated by changes in pH_i and V_m.

A Calibrated V_m (left) and pH_i (right) changes and Ca^{2+} signals (middle) evoked by resact.

B Normalized V_m, pH_i, and Ca^{2+} signals evoked by 10 pM resact; the first 600 ms after mixing are shown. The hyperpolarization precedes the pH_i increase, whereas the pH_i increase precedes the Ca^{2+} increase.

C Latency of the V_m, the pH_i, and the Ca^{2+} signals evoked by various resact concentrations (mean ± SD; $n = 3$).

D Normalized pH_i and Ca^{2+} signals evoked by photorelease of cGMP in sperm loaded with caged cGMP.

E Calibrated V_m and Ca^{2+} signals evoked by 1 nM resact; the threshold voltage (V_{thr}) for the Ca^{2+} influx was deduced from the latency of the Ca^{2+} signal.

F Calibrated pH_i and Ca^{2+} signals evoked by 1 nM resact; the threshold pH_i (pH_{thr}) at which the Ca^{2+} influx commences was deduced from the latency of the Ca^{2+} signal.

G Linear relationship between pH_{thr} and V_{thr} for activation of Ca^{2+} influx by various resact concentrations (data derived from Supplementary Fig S6; mean ± SD; $n \geq 3$).

was as follows: first sperm hyperpolarized, then the cytosol alkalized, and finally, Ca^{2+} commenced to rise (Fig 6B and C, Supplementary Fig S6). Furthermore, the pH_i increase evoked by intracellular photorelease of cGMP also preceded the onset of the Ca^{2+} signal (Fig 6D) (Darszon *et al*, 2008). These results are consistent with the notion that the resact-induced alkalization enables activation of CatSper channels upon depolarization.

From the latency of the Ca^{2+} signal at different resact concentrations, we identified pairs of voltage threshold (V_{thr}) and pH_{thr} at which the Ca^{2+} influx commenced (Fig 6E–G). For example, using 1 nM resact, Ca^{2+} influx commenced at V_{thr} of −71 ± 3 mV and at pH_{thr} of 7.36 ± 0.004 (Fig 6E–G, $n = 3$). For resact concentrations from 10 pM to 25 nM, the respective V_{thr} versus pH_{thr} pairs displayed an inverse, linear relationship (Fig 6G), i.e. with increasing resact concentrations, the Ca^{2+} influx commenced at more negative V_{thr} and at more alkaline pH_{thr} (Supplementary Fig S7). The slope of the straight line fitted to the data yielded a $\Delta V_{thr}/\Delta pH$ ratio of 75 mV. This result underscores the intimate relationship between pH_i and V_m for CatSper activation, which requires that changes in pH_i and V_m proceed in precise chronology. In mouse sperm, a change of pH_i from 6 to 7 shifts the voltage dependence of CatSper activation by about −70 mV (Kirichok *et al*, 2006), indicating that the pH_i sensitivity of mammalian and sea urchin CatSper is similar. In summary, our experiments indicate that the resact-induced alkalization is key to the Ca^{2+} influx via CatSper.

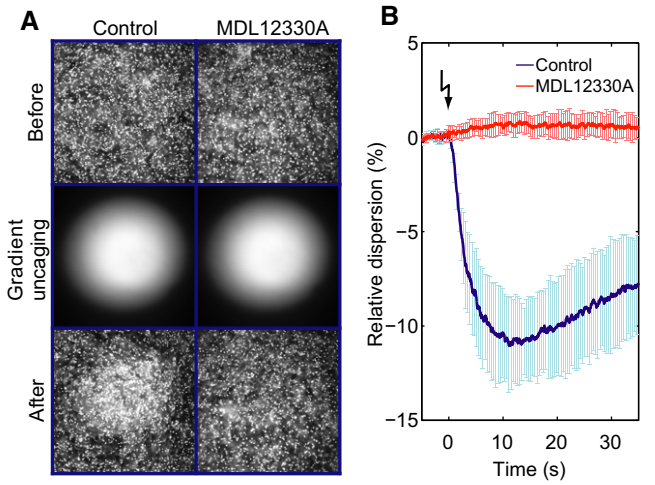

Figure 7. CatSper inhibitors abolish chemotaxis of sperm in an chemoattractant gradient.

A Dark-field microscopy images of a sperm suspension before (top) and after (bottom) photorelease of a resact gradient (middle) in the absence (control; left) or presence of the CatSper inhibitor MDL12330A (10 μM; right). MDL12330A abolishes resact-induced sperm accumulation.

B Relative change of the sperm dispersion in the field of view evoked by photorelease of resact (t = 0, flash) in the absence (control; blue) or presence of MDL12330A (red); a decrease in dispersion indicates sperm accumulation in the irradiated area (mean ± SD; n = 4).

We attempted to prevent the resact-induced alkalization by incubating sperm with the membrane-permeant pH buffer imidazole. Imidazole ≤ 20 mM attenuated the resact-induced alkalization in a dose-dependent fashion; at 30 mM imidazole, the alkalization was abolished (Supplementary Fig S8A). Concomitantly, the Ca^{2+} response was abolished as well (Supplementary Fig S8B), suggesting that the alkalization is required for CatSper activation. However, we observed that imidazole also strongly reduced the initial hyperpolarization (Supplementary Fig S8D and E), demonstrating that the drug is not suited to study signaling in sea urchin sperm. We wondered whether incubation with a physiological pH buffer like bicarbonate (HCO_3^-) prevents the pH_i responses—assuming that HCO_3^- enters the sperm. However, the resact-induced alkalization was similar in the absence and presence of 10 and 30 mM HCO_3^- (Supplementary Fig S8F).

CatSper controls chemotaxis of sperm

Finally, we tested whether CatSper controls chemotactic steering of sperm. In a shallow observation chamber under a dark-field microscope, sperm were bathed in caged resact (Kaupp *et al*, 2003; Böhmer *et al*, 2005; Alvarez *et al*, 2012). A resact gradient was established by photolysis of caged resact in the center of the recording chamber (Fig 7A). After the flash, sperm accumulated in the irradiated area, indicated by a decrease in sperm dispersion in the field of view, whereas the surrounding area became depleted of sperm (Fig 7, Supplementary Movies S1 and S2; control); MDL and mibefradil abolished the resact-induced accumulation of sperm (Fig 7, MDL12330A; Supplementary Movies S1 and S2). We conclude that the chemoattractant-induced Ca^{2+} influx via CatSper controls navigation of sperm in a resact gradient.

Discussion

Although CatSper has been discovered more than a decade ago and CatSper genes are present in many phyla, knowledge about CatSper channels originates exclusively from studies of human and mouse sperm. We show that CatSper constitutes the long-sought Ca^{2+} channel that controls chemotaxis in sea urchin sperm. Moreover, we unravel in quantitative terms the interplay between pH_i and V_m to control Ca^{2+} influx via CatSper in intact sperm.

At rest, V_{thr} of CatSper activation is slightly more positive than V_{rest} and the channel is closed. The chemoattractant-induced hyperpolarization (Fig 8B, black arrow) evokes a rapid intracellular alkalization via the sNHE exchanger that harbors a classic voltage-sensor motif, which probably mediates the voltage dependence (Wang *et al*, 2003; Nomura & Vacquier, 2006). The alkalization shifts the voltage dependence of CatSper by as much as 30 mV to more negative values (Fig 8B, blue arrow) and, thereby, enables CatSper to open during the subsequent depolarization brought about by hyperpolarization-activated and cyclic nucleotide-gated (HCN) channels (Fig 8B, red arrow) (Gauss *et al*, 1998; Galindo *et al*, 2005). The high cooperativity of the allosteric pH control serves as a sensitive mechanism that allows gating of CatSper within the operational voltage range set by V_{rest} (about −50 mV) and the reversal potential of the CNGK channel (about −95 mV).

In a chemical gradient, sperm are periodically stimulated with the angular frequency of circular swimming of ~1 Hz (Böhmer *et al*, 2005). The periodic stimulation can be emulated by repetitive (1 Hz) photorelease of cGMP; each cGMP pulse evokes a V_m and Ca^{2+} response of similar amplitude (Kashikar *et al*, 2012). We gained further insight into the interplay between pH_i and Ca^{2+} responses by studying pH_i signals evoked by repetitive photorelease of cGMP. Whereas the first flash produced a large increase of pH_i, subsequent flashes evoked only a small or no further alkalization (Fig 8C). Thus, once alkalization shifted the voltage dependence of CatSper to the permissive voltage range, channel gating is controlled by voltage only. This indicates that ΔpH_i is the mechanism that enables sperm to transduce periodic V_m changes into periodic Ca^{2+} changes during sperm navigation on periodic paths in a chemoattractant gradient (Kashikar *et al*, 2012).

Here, we reveal intriguing commonalities and differences between signaling pathways in sperm from mammals and marine invertebrates. Although distinct in many respects, signaling pathways share both CatSper and the sNHE exchanger (Fig 8A), suggesting that a voltage-induced change in pH_i and a pH-induced activation of CatSper are evolutionary conserved signaling events. A mechanism reminiscent of that controlling CatSper in sea urchins has recently been proposed for mouse sperm (Chavez *et al*, 2014). Hyperpolarization by Slo3, the principal K^+ channel in mouse (Santi *et al*, 2010; Zeng *et al*, 2011, 2013) and human sperm (Brenker *et al*, 2014), is required for CatSper to open upon depolarization. The hyperpolarization might involve alkalization, probably mediated by sNHE (Chavez *et al*, 2014). These events seem to control sperm capacitation, a maturation process inside the female genital tract. At first sight, these capacitation events are reminiscent of the hyperpolarization-induced events during chemotaxis in sea urchin sperm. However, the time scales are entirely different: Mammalian sperm capacitation proceeds in minutes to hours, whereas chemotactic signaling happens within subseconds. Finally, the

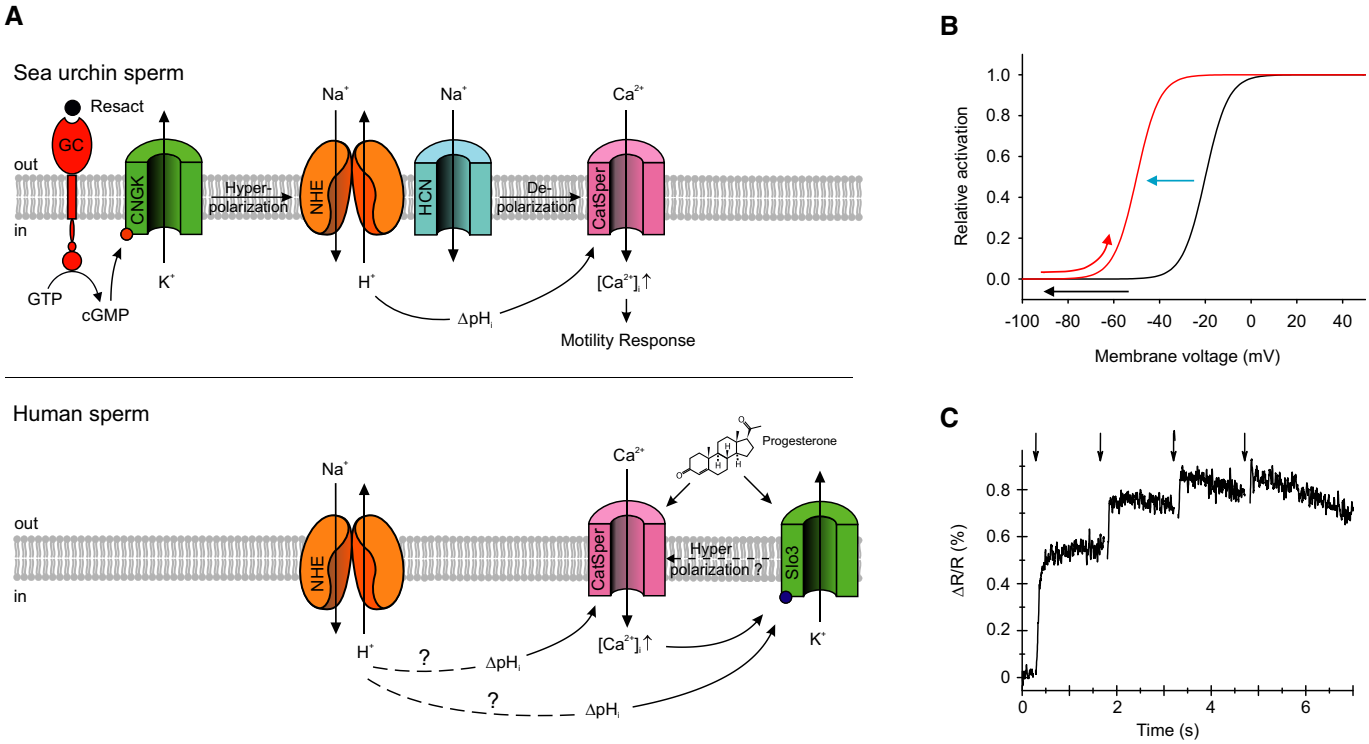

Figure 8. Role of CatSper in chemosensory signaling pathways of sea urchin and mammalian sperm.

A Signaling pathways in sperm of *A. punctulata* (upper panel) and humans (lower panel). Questionmarks above dashed lines in the lower panel indicate that the mechanism of how ΔpH_i is produced and the hyperpolarization by Slo3 has not been firmly established. Solid lines indicate that the action of ΔpH_i on CatSper and of ΔpH_i and Ca^{2+} on Slo3 activity has been firmly established.

B Model of the pH_i-induced change in the voltage dependence and V_{thr} of CatSper; the resact-induced hyperpolarization (black arrow) evokes a rapid alkalization that shifts the voltage dependence of CatSper activation to more negative values (blue arrow) and, thereby, primes CatSper to open during the subsequent depolarization (red arrow).

C Changes in pH_i evoked by repetitive release (arrows) of cGMP from caged cGMP. The first UV flash was delivered at $t = 0$.

physiological trigger for Slo3 activation and the precise interplay between V_m and pH_i to control mammalian CatSper are unknown. In conclusion, the allosteric mechanism of CatSper activation by pH_i and V_m in sea urchins provides a blueprint for studies in mammalian sperm.

On a final note, a difference between chemosensation in sea urchin and human sperm might concern the interplay of CatSper and K^+ channels (Fig 8A). In sea urchin, the opening of CNGK first activates sNHE and eventually CatSper. Thus, CNGK is located upstream of CatSper on the excitatory limb of the signaling pathway (Fig 8A). By contrast, in human sperm, Slo3 is activated by Ca^{2+} (Brenker *et al*, 2014), and a Ca^{2+}-induced hyperpolarization might curtail the progesterone-induced Ca^{2+} influx via CatSper. Thus, Slo3 is placed downstream of CatSper on the recovery limb of signaling (Fig 8A). This variation of signaling motifs might reflect a phylogenetic adaptation to the direct activation of human CatSper by extracellular ligands such as progesterone.

In conclusion, CatSper constitutes a crucial component of Ca^{2+} entry employed by diverse signaling pathways. In general, CatSper might serve as a versatile polymodal sensor that integrates multiple stimuli such as pH_i, female factors, and membrane voltage. Depending on the species, CatSper employs either intracellular alkalization or ligand binding to allosterically shift its voltage dependence to the permissive range of membrane potentials. We envisage that variations or combinations of these two mechanisms control CatSper in other species.

Materials and Methods

Arbacia punctulata sperm

Collection of dry sperm and composition of artificial seawater (ASW) was as described previously (Kaupp *et al*, 2003; Strünker *et al*, 2006; Kashikar *et al*, 2012). In brief, about 0.5 ml of 0.5 M KCl was injected into the body cavity to evoke spawning. Spawned sperm (dry sperm) were collected using a Pasteur pipette and stored on ice.

Cloning of *Ap*CatSper subunits

For cloning of *Ap*CatSper 2 and *Ap*CatSper 3, fragments of partial clones from orthologous *Strongylocentrotus purpuratus Sp*CatSper 2 and 3 (kindly provided by D. Ren, University of Pennsylvania, Philadelphia, USA) were amplified. For cloning of *Ap*CatSper 1 and *Ap*CatSper 4, we compared the sequences of mammalian CatSper 1 and 4 subunits with predicted messenger RNA (mRNA) sequences from the *S. purpuratus* genome project, and we designed primers to amplify fragments of *Sp*CatSper 1 and *Sp*CatSper 4 from a cDNA

library of *S. purpuratus* testis. The *Sp*CatSper 1–4 fragments were used as probes to screen random-primed cDNA libraries of *A. punctulata* testis under low-stringency conditions. Overlapping *Ap*CatSper partial clones were combined to yield full-length clones; missing sequence information at the 5′- and 3′-end was completed by RACE-PCR (Frohman *et al*, 1988). PCRs, the construction and screening of cDNA libraries, subcloning, and sequencing of cDNA were performed according to standard protocols. The *Ap*CatSper 2 and 3 clones were fused with the coding sequence for a C-terminal hemagglutinin tag (HA-tag) and cloned into the mammalian expression vector pcDNA3.1+ (Invitrogen).

Antibodies

The antibodies directed against the GC (GCN3D12) and the CNGK (AP47C9) were described previously (Bönigk *et al*, 2009; Pichlo *et al*, 2014). A monoclonal antibody from rat (RKKE4F6) was directed against the C-terminus (amino acids 297–317) of *Ap*CatSper 3. Another monoclonal antibody from rat (APCS28G4) was directed against the N-terminus of *Ap*CatSper 2 (amino acids 42–58). The rat anti-HA antibody was from Roche Applied Science. Secondary antibodies were used as follows: goat anti-rat-HRP antibody (Dianova); goat anti-rat-IRDye800cw antibody (LI-COR); donkey anti-rat-Cy3 (Dianova) and goat anti-rat-Alexa488 (Life Technologies).

Immunocytochemistry

Sperm were immobilized on SuperFrost Plus microscope slides (Menzel) and fixed for 5 min with 4% paraformaldehyde. After preincubation with 0.5% Triton X-100 and 5% chemiblocker (Millipore) in 0.1 M phosphate buffer (pH 7.4), sperm were incubated for 1 h with antibodies RKKE4F6 or AP47C9 (undiluted in the presence of 0.5% Triton X-100), or GCN3D12 (1:100 diluted in the presence of 0.5% Triton X-100) and visualized with the donkey anti-rat-Cy3 (RKKE4F6, GCN3D12) or goat anti-rat-Alexa488 (AP47C9) antibodies.

Western blotting

CHO cells transiently transfected with *Ap*CatSper 2 or *Ap*CatSper 3 were resuspended in phosphate-buffered saline (PBS) containing (in mM) 137 NaCl, 2.7 KCl, 6.5 Na_2HPO_4, 1.5 KH_2PO_4, pH 7.4, and the protease inhibitor Complete (Roche). Total protein content was determined by using the BCA Assay kit (Pierce). Ten μg of total protein was used in the Western blot analysis. Membrane proteins from *A. punctulata* sperm were prepared as previously described (Mengerink & Vacquier, 2004). Ten μg of membrane proteins was used in the Western blot analysis. Proteins were separated by 10% SDS–polyacrylamide gel electrophoresis (SDS–PAGE) and blotted, and the membranes were probed with RKKE4F6 (undiluted), APCS28G4 (dilution 1:100), or rat anti-HA (dilution 1:1,000). The goat anti-rat-HRP antibody (dilution 1:5,000) was used to visualize protein bands by a chemoluminescence detection kit; chemoluminescence was detected via a CCD-imaging system (LAS-3000; Fuji) (CHO proteins) or by hyperfilms (GE Healthcare) (sperm proteins). The goat anti-rat-IRDye800cw antibody (1:20,000) was used to visualize sperm protein bands via the Odyssey Imaging System (LI-COR).

Mass spectrometry of proteins from *A. punctulata* flagella

Sperm flagella and heads were separated as described (Mengerink & Vacquier, 2004; Strünker *et al*, 2006) with some modifications: Dry sperm was diluted (1:25) in ASW pH 7.8 and centrifuged (200 *g*, 7 min) to sediment coelomocytes. The supernatant was centrifuged (3,000 *g*, 15 min) to sediment sperm. The sperm pellet was diluted in ASW pH 7.8 with protease inhibitor Complete (Roche) (1:10 dilution). The sperm suspension was sheared ~20 times with a 24-G needle and centrifuged (800 *g*, 10 min) to sediment intact sperm and sperm heads. The purity of flagella preparations was checked by phase-contrast microscopy. Shearing and subsequent centrifugation was repeated several times until pure flagella samples were obtained. All steps were performed on ice. Flagella were lysed by several "freeze/thaw" cycles and sonification steps in buffer containing (in mM): 25 HEPES pH 7.5, 10 NaCl, 2 EGTA, and protease inhibitor cocktails (Roche Applied Science and Sigma). Membranes were sedimented by ultracentrifugation (100,000 *g*, 30 min, 4°C) and washed twice with 0.1 M $(NH_4)_2CO_3$. After another ultracentrifugation step, membrane pellets were resuspended, sonicated, and processed by tryptic in-solution digestion (sequencing grade modified trypsin, Promega) in a methanol and NH_4HCO_3 buffer (Fischer *et al*, 2006). After removal of membranes by ultracentrifugation, samples were desalted using Spec PT C18 AR tips (Varian). Both MudPIT (2D) with seven salt steps and one-dimensional (1D) analysis were performed on an LTQ Orbitrap Velos (Thermo Fisher Scientific) according to Fränzel *et al* (2010) and Trötschel *et al* (2012). All database searches were performed using SEQUEST algorithm, embedded in Proteome Discoverer™ (Rev. 1.2.0.208 or Rev. 1.4.0.288, Thermo Fischer Scientific). Searches were done by using both an *A. punctulata* protein database derived from testis transcriptome and sperm genome sequencing (to be published) and an NCBI protein database for *S. purpuratus* proteins, in which the *S. purpuratus* protein sequences for the CatSper subunits 1, 2, 3, 4, GC, and CNGK were replaced by the respective *A. punctulata* sequences. Tryptic peptides with ≤ 2 missed cleavages were accepted. Oxidation of methionine was permitted as variable modification. The mass tolerance for precursor ions was set to 6 ppm; the mass tolerance for fragment ions was set to 0.8 amu. For search result filtering, a false discovery rate (FDR) of $< 1\%$ was applied, and ≥ 2 peptides per protein as well as peptides with search result rank 1 were required.

Co-immunoprecipitation

The monoclonal rat anti-*Ap*CatSper 2 and anti-*Ap*CatSper 3 antibodies APCS28G4 and RKKE4F6, respectively, were immobilized on Protein G Sepharose 4 Fast Flow (GE Healthcare). *Arbacia punctulata* dry sperm were suspended in lysis buffer containing in mM: 140 NaCl, 1 EDTA, 1% *n*-dodecyl-β-D-maltopyranoside (DDM, Anatrace), 10 Tris–HCl (pH 7.6), and protease inhibitor cocktail (Sigma). The suspension (total lysate) was centrifuged for 10 min at 10,000 × *g*, and the total protein content of the supernatant, containing cytosolic and solubilized membrane proteins, was determined by a BCA Assay kit (Pierce). For co-immunoprecipitation, proteins (input) were pre-incubated with fresh Protein G resin end-over-end for 30 min at 4°C. The suspension was briefly centrifuged

(0.5 min, 200 × *g*, 4°C), and the supernatant was added to the respective antibody-coupled resin, incubated end-over-end overnight at 4°C, and centrifuged to remove the supernatant (flow through). The resin was subsequently washed five times with lysis buffer; finally, co-immunoprecipitated proteins were eluted with 1× SDS–PAGE sample buffer (2% [w/v] SDS, 50 mM Tris, 12.5% glycerin, 1% 2-mercaptoethanol, 0.01% bromphenol blue). For Western blot analysis, proteins were separated by 10% SDS–PAGE and blotted, and membranes were probed with either the anti-*Ap*CatSper 2 or anti-*Ap*CatSper 3 (both undiluted) antibody and visualized, using the Odyssey Imaging System (LI-COR).

For mass spectrometry analysis, (co-)immunoprecipitated proteins were separated by 10% SDS–PAGE. Gels were stained with colloidal Coomassie, containing 0.08% (w/v) Coomassie G-250, 1.6% (v/v) phosphoric acid, 8% (w/v) ammonium sulfate, and 20% (v/v) methanol, destained with 1% (v/v) acetic acid, and cut into 10 slices. Proteins in the slices were processed by tryptic in-gel digestion and analyzed by protein mass spectrometry.

Measurement of changes in intracellular Ca^{2+} concentration, pH, and membrane voltage

We measured changes in $[Ca^{2+}]_i$, pH_i, and V_m in a rapid-mixing device (SFM-400; BioLogic) in the stopped-flow mode. The changes in $[Ca^{2+}]_i$, pH_i, and V_m were measured with the Ca^{2+} indicator Fluo-4-AM, the pH indicator BCECF-AM, and the voltage-sensitive indicator di-8-ANEPPS (Molecular Probes), respectively (Solzin *et al*, 2004; Strünker *et al*, 2006; Bönigk *et al*, 2009; Kashikar *et al*, 2012). Dry sperm were suspended 1:6 (vol/vol) in loading buffer containing ASW and the indicator in the absence (BCECF-AM) or presence (Fluo-4-AM, di-8-ANEPPS) of 0.5% Pluronic F127 (Sigma-Aldrich or Molecular Probes). After incubation (for 45–120 min with Fluo-4-AM, 10–15 min for BCECF-AM, or 5 min for di-8-ANEPPS) at 17°C, the sample was diluted 1:20 to 1:200 with ASW. Sperm were allowed to equilibrate in the new medium for 5 min. In the stopped-flow device, the sperm suspension was rapidly mixed 1:1 (vol/vol) with the respective stimulus. Concentrations of inhibitors or ligands are given as final concentrations after mixing. Fluorescence was excited by a 150-W Xe lamp (LSB521; LOT Oriel) or a SpectraX Light Engine (Lumencor). Emission was recorded by photomultiplier modules (H9656-20; Hamamatsu Photonics). The signal was amplified and filtered through a voltage amplifier (DLPVA-100-B-S; Femto Messtechnik). Data acquisition was performed with a data acquisition pad (PCI-6221; National Instruments) and Bio-Kine software (BioLogic). For Ca^{2+} and V_m recordings, the excitation light was passed through either an ET490/20 nm (Chroma Technology) (Xe lamp) or a BrightLine 475/28-nm filter (Semrock) (SpectraX Light Engine). For pH_i measurements, the excitation light was passed through a BrightLine 452/45-nm filter (Semrock). For Ca^{2+} measurements, the emitted light was passed through a BrightLine 536/40 filter (Semrock). Ca^{2+} signals represent the average of at least two recordings and are depicted as the percent change in fluorescence (ΔF) with respect to the mean of the first 5–10 data points before the onset of the signal (F_0). The control (ASW) $\Delta F/F_0$ signal was subtracted from the NH_4Cl-, pH_i-clamp-, resact-, or cGMP-induced signals. The V_m signals were recorded in the ratiometric dual-emission mode. The filters in front of the two photomultipliers were BrightLine 536/40 nm and BrightLine 628/40 (Semrock). The BioLogic software was used to record fluorescence in the dual-emission mode. The V_m signals represent the ratio F536/628 (R). The control (ASW) R signal was subtracted from the resact- or cGMP-induced signals. The mean R of the first 5–10 data points before the onset of the changes in fluorescence was set to 0, yielding ΔR. The V_m signals represent the average of at least three recordings and were digitally smoothed with five-point average smoothing. The changes in di-8-ANEPPS fluorescence were calibrated to yield V_m values (mV) by mixing sperm with both resact (2 nM) and various $[K^+]_o$ (Strünker *et al*, 2006). With increasing $[K^+]_o$, the amplitude of the resact-induced hyperpolarization decreases and, eventually, sperm depolarized. Plotting the resact-evoked ΔR versus $[K^+]_o$ allows interpolation of the $[K^+]_o$ at which resact does not change V_m. At this $[K^+]_o$ null-point, the Nernst potential of K^+ equaled V_{rest} before stimulation. We calculated the respective Nernst potential, assuming an intracellular K^+ concentration of 423 mM. Moreover, ΔR is linearly related to $[K^+]_o$, which allows to determine ΔR/mV. Determination of V_{rest} and calibration of ΔR into mV was performed for each set of experiments. BCECF fluorescence was recorded in a dual-emission mode using BrightLine 494/20-nm and BrightLine 540/10-nm filters (Semrock). The pH_i signals represent the ratio of F494/540, represent the average of at least two recordings, and are depicted as the percent of the relative change in ratio ($\Delta R/R$) with respect to the mean of the first 5–10 data points before the onset of the signal. The control (ASW) signal was subtracted from the NH_4Cl-, pH_i-clamp-, resact-, or cGMP-induced signals.

The calibration procedure for BCECF fluorescence to yield pH_i by the pH_i-null-point method is described in the result section and below; pH_i calibration was performed for each set of experiments. The pH_i-null-point solutions were prepared according to the following equation: $pH_i\text{-null} = pH_o - 0.5 \log([TMA]/[BA])$; pH_o = extracellular pH (7.8) (Eisner *et al*, 1989), wherein [TMA] indicates the concentration of trimethylamine and [BA] that of butyric acid. According to this equation, each [TMA]/[BA] ratio defines a new pH_i or pH_i-null-point. When a cell with a resting pH_i (pH_{rest}) is placed in a pH_i-null-point solution, it will not change its pH_i when the pH_i-null-point solution matches pH_{rest}. If the null-point is more alkaline than pH_{rest}, the cell will alkalize; if the null-point is more acidic, then the cell will acidify. Monitoring the changes in pH_i after mixing sperm with various null-point solutions allows interpolating pH_{rest}. When the pH_i-null-point does not match pH_{rest}, the absolute concentrations of acid and base determine to what extent the pH_i of a cell will change (Chow *et al*, 1996): The higher the concentrations of the acid/base mixture, the more the pH_i will be shifted toward the pH_i-null-point. At saturation, the newly established pH_i matches the pH_i-null-point; thus, the cell is clamped to a new pH_i. Therefore, we refer to this saturating pH_i-null-point solution as pH_i-clamp solution. Finally, the time course of pH_i determines the time window for which this pH_i-clamp concept holds. To ensure that in *A. punctulata* sperm, the pH_i was indeed clamped to the pH_i-null-point for several tens of seconds, we determined for each pH_i-null-point solution, i.e. for each TMA/BA ratio, the molar concentrations of TMA and BA required to produce saturating changes in pH_i (Supplementary Fig S9). The pH_i-clamp solutions that clamped pH_i in *A. punctulata* sperm to pH_i-null all contained 60 mM BA, whereas the TMA concentration was varied to yield the respective pH_i-null; for example, for the pH_i-null 7.0 solution, we used 1.5071 mM TMA/60 mM BA, for the pH_i-null 7.2 solution, 3.7857 mM TMA/60 mM BA, etc.

Addition of TMA and BA increased the osmolarity of the ASW by < 13%.

Caged compounds and flash photolysis

DEACM-caged cGMP and DMNB-caged resact were obtained from V. Hagen (Leibniz-Institut für Molekulare Pharmakologie, Berlin) (Hagen *et al*, 2003; Kaupp *et al*, 2003). For Ca^{2+} recordings, sperm were diluted 1:6 in loading buffer (ASW) containing Fluo-4-AM and 30 μM DEACM-caged cGMP for ≥ 45 min (Kaupp *et al*, 2003). For pH_i recordings, sperm were incubated first with 30 μM DEACM-caged cGMP for ≥ 40 min followed by incubation for another 10–15 min with BCECF-AM. After loading, sperm were diluted 1:20 to 1:200 for stopped-flow experiments. For experiments with DMNB-caged resact, sperm were first loaded with Fluo-4-AM; after loading, the sample was diluted 1:20 to 1:200 with ASW containing 1 μM DMNB-caged resact. Sperm were allowed to equilibrate in the new medium for 5 min. In the stopped-flow device, the sperm suspension was rapidly mixed 1:1 (vol/vol) with ASW (control) or the respective inhibitors. About 2–5 s after mixing, caged cGMP and caged resact were photolyzed by a UV flash (~1 ms) from a Xenon flash lamp (JML-C2; Rapp OptoElectronic). The UV flash was passed through a bandpass 295- to 395-nm interference filter (Rapp OptoElectronic) and delivered by a liquid light guide to the cuvette (FC-15; BioLogic) of the stopped-flow device.

Sperm chemotaxis

Sperm accumulation in a resact gradient was studied as described with some modifications (Alvarez *et al*, 2012; Hirohashi *et al*, 2013). In brief, sperm swimming in a recording chamber (150 μm depth) were imaged using a microscope (IX71; Olympus) equipped with a 10× objective (UPlanSApo; NA 0.4; Olympus). Stroboscopic dark-field illumination (2 ms pulses) was achieved using a white LED (K2 star; Luxeon), a custom-made housing, and a pulse generator. Images were bandpass-filtered (HQ520/40; Chroma) and acquired at 20 Hz, using an electron-multiplying charge-coupled device camera (DU-897D; Andor). Sperm were suspended at about 10^8 cells/ml in ASW containing caged resact (50 nM; control) or caged resact and MDL 12330A (10 μM) or mibefradil (60 μM). Resact was released by 400-ms UV flashes (LED M365L2-C1; Thorlabs) with a Gaussian profile of σ = 178 μm width, coupled to the microscope using a beam splitter (495 nm cutoff, BrightLine; Semrock). The light power delivered to the sample was 1.7 mW. The sperm distribution around the center of the illuminated area was quantified by the relative changes of the weighted standard distance (Alvarez *et al*, 2012; Hirohashi *et al*, 2013). Only points within a distance $\leq 2\sigma$ to the center of the UV flash were considered. The uncaging gradient was quantified by imaging fluorescein (10 μM) with the same UV light source and optical components.

Data analysis

The data obtained from the stopped-flow recordings were analyzed using Prism 5 (GraphPad Software) and OriginPro 8.1G SR3 (OriginLab Corporation). All data are given as mean ± standard deviation.

Supplementary information for this article is available online: http://emboj.embopress.org

Acknowledgements

We thank K.M. Dressler and Rene Pascal for technical assistance, H. Krause for preparing the manuscript, and D. Ren (University of Pennsylvania, Philadelphia, USA) for providing us with the *S. purpuratus* cDNA clones encoding CatSper 2 and CatSper 3. This work was supported by the German Research Foundation (SFB645).

Author contributions

RS and TS conceived the project. RS, MF, WB, LA, CT, AP, AM, NG, PP, NDK, EK, JJ, BT, HK, DF, FW, UBK, and TS designed and performed experiments. TS, RS, and UBK wrote the manuscript. All authors revised the manuscript.

Conflict of interest

The authors declare that they have no conflict of interest.

References

Aitken RJ, Kelly RW (1985) Analysis of the direct effects of prostaglandins on human sperm function. *J Reprod Fertil* 73: 139 – 146

Alasmari W, Costello S, Correia J, Oxenham SK, Morris J, Fernandes L, Ramalho-Santos J, Kirkman-Brown J, Michelangeli F, Publicover S, Barratt CL (2013) Ca^{2+} signals generated by CatSper and Ca^{2+} stores regulate different behaviors in human sperm. *J Biol Chem* 288: 6248 – 6258

Alvarez L, Dai L, Friedrich BM, Kashikar ND, Gregor I, Pascal R, Kaupp UB (2012) The rate of change in Ca^{2+} concentration controls sperm chemotaxis. *J Cell Biol* 196: 653 – 663

Alvarez L, Friedrich BM, Gompper G, Kaupp UB (2014) The computational sperm cell. *Trends Cell Biol* 24: 198 – 207

Avenarius MR, Hildebrand MS, Zhang Y, Meyer NC, Smith LL, Kahrizi K, Najmabadi H, Smith RJ (2009) Human male infertility caused by mutations in the CATSPER1 channel protein. *Am J Hum Genet* 84: 505 – 510

Babcock DF, Bosma MM, Battaglia DE, Darszon A (1992) Early persistent activation of sperm K^+ channels by the egg peptide speract. *Proc Natl Acad Sci USA* 89: 6001 – 6005

Baldi E, Luconi M, Muratori M, Marchiani S, Tamburrino L, Forti G (2009) Nongenomic activation of spermatozoa by steroid hormones: facts and fictions. *Mol Cell Endocrinol* 308: 39 – 46

Beltrán C, Zapata O, Darszon A (1996) Membrane potential regulates sea urchin sperm adenylylcyclase. *Biochemistry* 35: 7591 – 7598

Bentley JK, Tubb DJ, Garbers DL (1986) Receptor-mediated activation of spermatozoan guanylate cyclase. *J Biol Chem* 261: 14859 – 14862

Bentley JK, Khatra AS, Garbers DL (1988) Receptor-mediated activation of detergent-solubilized guanylate cyclase. *Biol Reprod* 39: 639 – 647

Böhmer M, Van Q, Weyand I, Hagen V, Beyermann M, Matsumoto M, Hoshi M, Hildebrand E, Kaupp UB (2005) Ca^{2+} spikes in the flagellum control chemotactic behavior of sperm. *EMBO J* 24: 2741 – 2752

Bond J, Varley J (2005) Use of flow cytometry and SNARF to calibrate and measure intracellular pH in NS0 cells. *Cytometry A* 64: 43 – 50

Bönigk W, Loogen A, Seifert R, Kashikar N, Klemm C, Krause E, Hagen V, Kremmer E, Strünker T, Kaupp UB (2009) An atypical CNG channel activated by a single cGMP molecule controls sperm chemotaxis. *Sci Signal* 2: ra68

Brenker C, Goodwin N, Weyand I, Kashikar ND, Naruse M, Krähling M, Müller A, Kaupp UB, Strünker T (2012) The CatSper channel: a polymodal chemosensor in human sperm. *EMBO J* 31: 1654 – 1665

Brenker C, Zhou Y, Müller A, Echeverry FA, Trötschel C, Poetsch A, Xia XM, Bönigk W, Lingle CJ, Kaupp UB, Strünker T (2014) The Ca^{2+}-activated K^+ current of human sperm is mediated by Slo3. *eLife* 3: e01438

Cai X, Clapham DE (2008) Evolutionary genomics reveals lineage-specific gene loss and rapid evolution of a sperm-specific ion channel complex: CatSpers and CatSperbeta. *PLoS ONE* 3: e3569

Chavez JC, Ferreira Gregorio J, Butler A, Trevino CL, Darszon A, Salkoff L, Santi CM (2014) SLO3 K+ channels control calcium entry through CATSPER channels in sperm. *J Biol Chem* 289: 32266 – 32275

Chow S, Hedley D, Tannock I (1996) Flow cytometric calibration of intracellular pH measurements in viable cells using mixtures of weak acids and bases. *Cytometry* 24: 360 – 367

Chung JJ, Navarro B, Krapivinsky G, Krapivinsky L, Clapham DE (2011) A novel gene required for male fertility and functional CATSPER channel formation in spermatozoa. *Nat Commun* 2: 153

Chung JJ, Shim SH, Everley RA, Gygi SP, Zhuang X, Clapham DE (2014) Structurally distinct Ca^{2+} signaling domains of sperm flagella orchestrate tyrosine phosphorylation and motility. *Cell* 157: 808 – 822

Cook SP, Babcock DF (1993) Selective modulation by cGMP of the K^+ channel activated by speract. *J Biol Chem* 268: 22402 – 22407

Dangott LJ, Garbers DL (1984) Identification and partial characterization of the receptor for speract. *J Biol Chem* 259: 13712 – 13716

Dangott LJ, Jordan JE, Bellet RA, Garbers DL (1989) Cloning of the mRNA for the protein that crosslinks to the egg peptide speract. *Proc Natl Acad Sci USA* 86: 2128 – 2132

Darszon A, Guerrero A, Galindo BE, Nishigaki T, Wood CD (2008) Sperm-activating peptides in the regulation of ion fluxes, signal transduction and motility. *Int J Dev Biol* 52: 595 – 606

Eisenbach M, Giojalas LC (2006) Sperm guidance in mammals – an unpaved road to the egg. *Nat Rev Mol Cell Biol* 7: 276 – 285

Eisner DA, Kenning NA, O'Neill SC, Pocock G, Richards CD, Valdeolmillos M (1989) A novel method for absolute calibration of intracellular pH indicators. *Pflugers Arch* 413: 553 – 558

Fischer F, Wolters D, Rogner M, Poetsch A (2006) Toward the complete membrane proteome: high coverage of integral membrane proteins through transmembrane peptide detection. *Mol Cell Proteomics* 5: 444 – 453

Florman HM, Jungnickel MK, Sutton KA (2008) Regulating the acrosome reaction. *Int J Dev Biol* 52: 503 – 510

Fränzel B, Trötschel C, Ruckert C, Kalinowski J, Poetsch A, Wolters DA (2010) Adaptation of *Corynebacterium glutamicum* to salt-stress conditions. *Proteomics* 10: 445 – 457

Frohman MA, Dush MK, Martin GR (1988) Rapid production of full-length cDNAs from rare transcripts: amplification using a single gene-specific oligonucleotide primer. *Proc Natl Acad Sci USA* 85: 8998 – 9002

Galindo BE, Neill AT, Vacquier VD (2005) A new hyperpolarization-activated, cyclic nucleotide-gated channel from sea urchin sperm flagella. *Biochem Biophys Res Commun* 334: 96 – 101

Galindo BE, de la Vega-Beltrán JL, Labarca P, Vacquier VD, Darszon A (2007) Sp-tetraKCNG: a novel cyclic nucleotide gated K^+ channel. *Biochem Biophys Res Commun* 354: 668 – 675

Gauss R, Seifert R, Kaupp UB (1998) Molecular identification of a hyperpolarization-activated channel in sea urchin sperm. *Nature* 393: 583 – 587

Gonzáles-Martínez MT, Guerrero A, Morales E, de De la Torre L, Darszon A (1992) A depolarization can trigger Ca^{2+} uptake and the acrosome reaction when preceded by a hyperpolarization in *L. pictus* sea urchin sperm. *Dev Biol* 150: 193 – 202

Guerrero A, García L, Zapata O, Rodríguez E, Darszon A (1998) Acrosome reaction inactivation in sea urchin sperm. *Biochim Biophys Acta* 1401: 329 – 338

Guerrero A, Nishigaki T, Carneiro J, Yoshiro T, Wood CD, Darszon A (2010a) Tuning sperm chemotaxis by calcium burst timing. *Dev Biol* 344: 52 – 65

Guerrero A, Wood CD, Nishigaki T, Carneiro J, Darszon A (2010b) Tuning sperm chemotaxis. *Biochem Soc Trans* 38: 1270 – 1274

Hagen V, Frings S, Wiesner B, Helm S, Kaupp UB, Bendig J (2003) [7-(Dialkylamino)coumarin-4-yl]methyl-caged compounds as ultrafast and effective long-wavelength phototriggers of 8-bromo-substituted cyclic nucleotides. *Chembiochem* 4: 434 – 442

Hildebrand MS, Avenarius MR, Fellous M, Zhang Y, Meyer NC, Auer J, Serres C, Kahrizi K, Najmabadi H, Beckmann JS, Smith RJ (2010) Genetic male infertility and mutation of CATSPER ion channels. *Eur J Hum Genet* 18: 1178 – 1184

Hirohashi N, Alvarez L, Shiba K, Fujiwara E, Iwata Y, Mohri T, Inaba K, Chiba K, Ochi H, Supuran CT, Kotzur N, Kakiuchi Y, Kaupp UB, Baba SA (2013) Sperm from sneaker male squids exhibit chemotactic swarming to CO_2. *Curr Biol* 23: 775 – 781

Ho H-C, Suarez SS (2001) Hyperactivation of mammalian spermatozoa: function and regulation. *Reproduction* 122: 519 – 526

Ho K, Wolff CA, Suarez SS (2009) CatSper-null mutant spermatozoa are unable to ascend beyond the oviductal reservoir. *Reprod Fertil Dev* 21: 345 – 350

Kashikar ND, Alvarez L, Seifert R, Gregor I, Jäckle O, Beyermann M, Krause E, Kaupp UB (2012) Temporal sampling, resetting, and adaptation orchestrate gradient sensing in sperm. *J Cell Biol* 198: 1075 – 1091

Kaupp UB, Solzin J, Hildebrand E, Brown JE, Helbig A, Hagen V, Beyermann M, Pampaloni F, Weyand I (2003) The signal flow and motor response controling chemotaxis of sea urchin sperm. *Nat Cell Biol* 5: 109 – 117

Kaupp UB, Kashikar ND, Weyand I (2008) Mechanisms of sperm chemotaxis. *Annu Rev Physiol* 70: 93 – 117

Kaupp UB (2012) 100 years of sperm chemotaxis. *J Gen Physiol* 140: 583 – 586

Kirichok Y, Navarro B, Clapham DE (2006) Whole-cell patch-clamp measurements of spermatozoa reveal an alkaline-activated Ca^{2+} channel. *Nature* 439: 737 – 740

Kirkman-Brown JC, Smith DJ (2011) Sperm motility: is viscosity fundamental to progress? *Mol Hum Reprod* 17: 539 – 544

Lee HC (1984a) A membrane potential-sensitive Na^+-H^+ exchange system in flagella isolated from sea urchin spermatozoa. *J Biol Chem* 259: 15315 – 15319

Lee HC (1984b) Sodium and proton transport in flagella isolated from sea urchin spermatozoa. *J Biol Chem* 259: 4957 – 4963

Lee HC, Garbers DL (1986) Modulation of the voltage-sensitive Na^+/H^+ exchange in sea urchin spermatozoa through membrane potential changes induced by the egg peptide speract. *J Biol Chem* 261: 16026 – 16032

Lishko PV, Botchkina IL, Fedorenko A, Kirichok Y (2010) Acid extrusion from human spermatozoa is mediated by flagellar voltage-gated proton channel. *Cell* 140: 327 – 337

Lishko PV, Botchkina IL, Kirichok Y (2011) Progesterone activates the principal Ca^{2+} channel of human sperm. *Nature* 471: 387 – 391

Liu J, Xia J, Cho KH, Clapham DE, Ren D (2007) CatSperbeta, a novel transmembrane protein in the CatSper channel complex. *J Biol Chem* 282: 18945 – 18952

Lobley A, Pierron V, Reynolds L, Allen L, Michalovich D (2003) Identification of human and mouse CatSper3 and CatSper4 genes: characterisation of a

common interaction domain and evidence for expression in testis. *Reprod Biol Endocrinol* 1: 53

Mengerink KJ, Vacquier VD (2004) Isolation of sea urchin sperm plasma membranes. *Methods Mol Biol* 253: 141 – 150

Miki K, Clapham DE (2013) Rheotaxis guides Mammalian sperm. *Curr Biol* 23: 443 – 452

Navarro B, Kirichok Y, Chung JJ, Clapham DE (2008) Ion channels that control fertility in mammalian spermatozoa. *Int J Dev Biol* 52: 607 – 613

Nishigaki T, Zamudio FZ, Possani LD, Darszon A (2001) Time-resolved sperm responses to an egg peptide measured by stopped-flow fluorometry. *Biochem Biophys Res Commun* 284: 531 – 535

Nomura M, Vacquier VD (2006) Proteins associated with soluble adenylyl cyclase in sea urchin sperm flagella. *Cell Motil Cytoskeleton* 63: 582 – 590

Oren-Benaroya R, Orvieto R, Gakamsky A, Pinchasov M, Eisenbach M (2008) The sperm chemoattractant secreted from human cumulus cells is progesterone. *Hum Reprod* 23: 2339 – 2345

Pichlo M, Bungert-Plumke S, Weyand I, Seifert R, Bonigk W, Strunker T, Kashikar ND, Goodwin N, Muller A, Pelzer P, Van Q, Enderlein J, Klemm C, Krause E, Trotschel C, Poetsch A, Kremmer E, Kaupp UB (2014) High density and ligand affinity confer ultrasensitive signal detection by a guanylyl cyclase chemoreceptor. *J Cell Biol* 206: 541 – 557

Publicover SJ, Giojalas LC, Teves ME, de Oliveira GS, Garcia AA, Barratt CL, Harper CV (2008) Ca^{2+} signalling in the control of motility and guidance in mammalian sperm. *Front Biosci* 13: 5623 – 5637

Qi H, Moran MM, Navarro B, Chong JA, Krapivinsky G, Krapivinsky L, Kirichok Y, Ramsey IS, Quill TA, Clapham DE (2007) All four CatSper ion channel proteins are required for male fertility and sperm cell hyperactivated motility. *Proc Natl Acad Sci USA* 104: 1219 – 1223

Quill TA, Ren D, Clapham D, Garbers DL (2001) A voltage-gated ion channel expressed specifically in spermatozoa. *Proc Natl Acad Sci USA* 98: 12527 – 12531

Ren D, Navarro B, Perez G, Jackson AC, Hsu S, Shi Q, Tilly JL, Clapham DE (2001) A sperm ion channel required for sperm motility and male fertility. *Nature* 413: 603 – 609

Reynaud E, de De la Torre L, Zapata O, Liévano A, Darszon A (1993) Ionic bases of the membrane potential and intracellular pH changes induced by speract in swollen sea urchin sperm. *FEBS Lett* 329: 210 – 214

Santi CM, Martinez-Lopez P, de la Vega-Beltran JL, Butler A, Alisio A, Darszon A, Salkoff L (2010) The SLO3 sperm-specific potassium channel plays a vital role in male fertility. *FEBS Lett* 584: 1041 – 1046

Schiffer C, Müller A, Egeberg DL, Alvarez L, Brenker C, Rehfeld A, Frederiksen H, Wäschle B, Kaupp UB, Balbach M, Wachten D, Skakkebaek NE, Almstrup K, Strünker T (2014) Direct action of endocrine disrupting chemicals on human sperm. *EMBO Rep* 15: 758 – 765

Shimomura H, Garbers DL (1986) Differential effects of resact analogues on sperm respiration rates and cyclic nucleotide concentrations. *Biochemistry* 25: 3405 – 3410

Smith JF, Syritsyna O, Fellous M, Serres C, Mannowetz N, Kirichok Y, Lishko PV (2013) Disruption of the principal, progesterone-activated sperm Ca^{2+} channel in a CatSper2-deficient infertile patient. *Proc Natl Acad Sci USA* 110: 6823 – 6828

Solzin J, Helbig A, Van Q, Brown JE, Hildebrand E, Weyand I, Kaupp UB (2004) Revisiting the role of H^+ in chemotactic signaling of sperm. *J Gene Physiol* 124: 115 – 124

Strünker T, Weyand I, Bönigk W, Van Q, Loogen A, Brown JE, Kashikar N, Hagen V, Krause E, Kaupp UB (2006) A K^+ -selective cGMP-gated ion channel controls chemosensation of sperm. *Nat Cell Biol* 8: 1149 – 1154

Strünker T, Goodwin N, Brenker C, Kashikar ND, Weyand I, Seifert R, Kaupp UB (2011) The CatSper channel mediates progesterone-induced Ca^{2+} influx in human sperm. *Nature* 471: 382 – 386

Suarez SS, Pacey AA (2006) Sperm transport in the female reproductive tract. *Hum Reprod Update* 12: 23 – 37

Suarez SS (2008) Regulation of sperm storage and movement in the mammalian oviduct. *Int J Dev Biol* 52: 455 – 462

Swietach P, Tiffert T, Mauritz JM, Seear R, Esposito A, Kaminski CF, Lew VL, Vaughan-Jones RD (2010) Hydrogen ion dynamics in human red blood cells. *J Physiol* 588: 4995 – 5014

Tavares RS, Mansell S, Barratt CL, Wilson SM, Publicover SJ, Ramalho-Santos J (2013) p,p′-DDE activates CatSper and compromises human sperm function at environmentally relevant concentrations. *Hum Reprod* 28: 3167 – 3177

Teves ME, Guidobaldi HA, Unates DR, Sanchez R, Miska W, Publicover SJ, Morales Garcia AA, Giojalas LC (2009) Molecular mechanism for human sperm chemotaxis mediated by progesterone. *PLoS ONE* 4: e8211

Trötschel C, Albaum SP, Wolff D, Schröder S, Goesmann A, Nattkemper TW, Poetsch A (2012) Protein turnover quantification in a multilabeling approach: from data calculation to evaluation. *Mol Cell Proteomics* 11: 512 – 526

Wang D, King SM, Quill TA, Doolittle LK, Garbers DL (2003) A new sperm-specific Na^+/H^+ exchanger required for sperm motility and fertility. *Nat Cell Biol* 5: 1117 – 1122

Wang H, Liu J, Cho KH, Ren D (2009) A novel, single, transmembrane protein CATSPERG is associated with CATSPER1 channel protein. *Biol Reprod* 81: 539 – 544

Wood CD, Nishigaki T, Furuta T, Baba SA, Darszon A (2005) Real-time analysis of the role of Ca^{2+} in flagellar movement and motility in single sea urchin sperm. *J Cell Biol* 169: 725 – 731

Zeng XH, Yang C, Kim ST, Lingle CJ, Xia XM (2011) Deletion of the Slo3 gene abolishes alkalization-activated K^+ current in mouse spermatozoa. *Proc Natl Acad Sci USA* 108: 5879 – 5884

Zeng XH, Navarro B, Xia XM, Clapham DE, Lingle CJ (2013) Simultaneous knockout of Slo3 and CatSper1 abolishes all alkalization- and voltage-activated current in mouse spermatozoa. *J Gene Physiol* 142: 305 – 313

